Progress In Electromagnetics Research M, Vol. 99, 35–44, 2021

A Meshless Method for TM Scattering from Arbitrary Shaped Radially Inhomogeneous Cylinders

Birol Aslanyürek[1, *] and Tolga U. Gürbüz[2]

Abstract—A meshless method for fast solution of the electromagnetic scattering problem related to arbitrary shaped radially inhomogeneous cylinders is proposed. This is an important problem since radially inhomogeneous circular cylinders are common in various engineering applications, and deformations such as notches, grooves, and noncircular holes on such cylinders are required for different purposes. This approach is basically an extension of the previously proposed method, which is based on Fourier series representation of the electric field on boundaries. In the original method, a multilayer cylinder with arbitrary shaped homogeneous layers is considered, and accordingly, the general solution of the cylindrical wave equation in homogeneous medium is used. Here we modify the method by considering the general solution in radially inhomogeneous medium and derive compact expressions for the field.

1. INTRODUCTION

Materials with continuous variation of material properties along a specific direction are called functionally graded materials (FGMs). Different types of FGMs are produced by processing various conventional materials, and due to their superior physical properties, they are used in a diverse range of applications [1].

A radially inhomogeneous cylinder whose material properties vary continuously along the radial direction only is a common example of FGM objects. The varying material properties of these cylinders may include the electrical properties. Efficient solution of the electromagnetic scattering problems related to such cases have been investigated for a long time and analytical solutions have been derived for special dielectric permittivity profiles in a number of studies [2–5]. In [6], these analytical solutions are used to solve the problem of oblique scattering from a possibly multilayer cylinder having radially inhomogeneous layers, by representing the problem as a system of coupled linear Volterra integral equations. For more general permittivity profiles, a finely stratified cylinder model, in which the radially inhomogeneous layer is assumed to be composed of concentric homogeneous layers, is applied in [7]. A meshless alternative based on Taylor's series expansion of the permittivity function is also proposed for such general profiles [8]. For the case that the permittivity changes not only along the radial direction but also along the azimuthal direction, an extension of the Rigorous Coupled Wave Analysis is applied to solve the scattering problem [9]. The radially inhomogeneous cylinders considered in all these studies have circular (or elliptical) cross sections. Circular FGM rods, which can be produced by using centrifugal methods [10], are examples of such cylinders. On the other hand, it is common to encounter engineering applications in which these circular rods are used as intermediate product. In such cases, for various purposes, they are processed in a way to create deformations, such as notches, grooves, and noncircular hollows, lying parallel to the axis of the cylinder. Hence, in this study we propose

Received 4 October 2020, Accepted 26 November 2020, Scheduled 29 November 2020

* Corresponding author: Birol Aslanyürek (baslan@yildiz.edu.tr).

[1] Department of Mathematical Engineering, Yildiz Technical University, Istanbul, Turkey. [2] Department of Computer Engineering, Gaziantep University, Gaziantep, Turkey.

a meshless method for fast computation of the field scattered from deformed radially inhomogeneous cylinders when the cylinder is normally illuminated by electromagnetic plane waves. To the best of our knowledge, except conventional discretization-based techniques such as Method of Moments (MoM) [11] or Finite Element Method (FEM) [12], this is the first method proposed for solution of the scattering problem related to arbitrary shaped radially inhomogeneous cylinders.

The approach given here is based on Fourier series representation of the electric field on boundaries, and it is basically an extension of the approach that we proposed in [13] for multilayer cylinders with arbitrary shaped homogeneous layers. In [13], the general solution of the cylindrical wave equation in homogeneous medium, i.e., a series of Hankel and Bessel functions, is used for each homogeneous layer. One might attempt to use these solutions for radially inhomogeneous cylinders by modeling the object as a multilayer cylinder composed of numerous thin homogeneous circular rings. However, regions near the arbitrary shaped boundary cannot be modeled by such rings. For this reason, here we need to modify the method in [13] by considering the general solution in a single-layer radially inhomogeneous medium instead of the series of Hankel and Bessel functions used in [13]. With the help of this modification, we derive compact expressions for the field. One can easily apply the proposed method for multilayer cylinders that have one or more radially inhomogeneous layers around a core.

In the Numerical Results Section, the proposed method is tested on radially inhomogeneous objects having two different cross-sections, i.e., a V-notched circle and a rectangle with a hole, which may be encountered in various applications [14, 15]. The numerical simulations performed for some basic permittivity profiles show that the proposed method yields accurate results in a short computing time compared to MoM.

Throughout the paper, the time dependency is assumed as $\exp(-i\omega t)$ and suppressed. Vectors and matrices are given in bold.

2. PROBLEM STATEMENT AND FORMULATION

Although there is no obstacle to using the method given in this paper for single layer radially inhomogeneous cylinders, here we deal with a two-layered cylindrical object composed of a radially inhomogeneous layer and a core layer as shown in Fig. 1 since in most applications there also exists a homogeneous core. We assume that the arbitrary shaped cylindrical object is infinitely long. When we consider the outermost medium as another layer and represent it by subscript 0, the complex permittivities of the layers from outside to inside are ε_0, $\varepsilon_1(\rho)$ and ε_2, where ρ is the radial coordinate. All layers are nonmagnetic and the corresponding wavenumbers are k_0, $k_1(\rho)$ and k_2. The boundaries between the layers are Γ_1 and Γ_2 which are defined by $\rho = f_1(\phi)$ and $\rho = f_2(\phi)$, respectively. Here, f_1 and f_2 are real single-valued functions in polar coordinates.

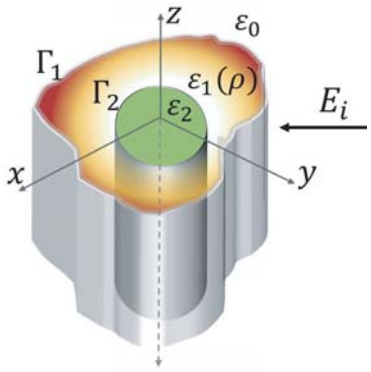

Figure 1. Arbitrary shaped radially inhomogeneous layer around a core.

The object is normally illuminated by a time-harmonic electromagnetic wave. The electric field of the incident wave is $\mathbf{E_i}(\rho, \phi) = u_i(\rho, \phi)\mathbf{e_z}$, where $\mathbf{e_z}$ is the unit vector in the z direction. In this case, the total field in the mth layer can be represented by scalar functions $u_m(\rho, \phi)$, $m = 0, 1, 2$. As shown in [5],

since ε_m is dependent only on ρ or is a constant, u_m can be represented as a series of two functions, namely $R_{n,m}^{(1)}$ and $R_{n,m}^{(2)}$, which are linearly independent solutions of

$$\left[\frac{1}{\rho}\frac{d}{d\rho}\left(\rho\frac{d}{d\rho}\right)+k_0^2\frac{\varepsilon_m(\rho)}{\varepsilon_0}-\frac{n^2}{\rho^2}\right]R_{n,m}^{(1),(2)}=0. \tag{1}$$

When ε_m is constant, i.e., the layer is homogeneous, it is known that the nth order Bessel function, $J_n(k_m\rho)$, and Hankel function of the first kind, $H_n^{(1)}(k_m\rho)$, are linearly independent solutions of Eq. (1). In [13] and its recursive version [16], the field is represented as a series of $J_n(k_m\rho)$ and $H_n^{(1)}(k_m\rho)$, and a fast approach is proposed for computation of the field scattered from arbitrary shaped homogeneous layers.

For various $\varepsilon_m(\rho)$ distributions, explicit expressions of $R_{n,m}^{(1)}$ and $R_{n,m}^{(2)}$ are also derived and used for computation of the field in several studies [2–5]. However, all boundaries are circular in these studies. In the present study, we propose an approach for computation of the field when the boundaries of radially inhomogeneous layers are arbitrary-shaped. This approach is basically an extension of the approach given in [13, 16] to the case that the arbitrary shaped layers can also be radially inhomogeneous. Accordingly, the field representation that is used in the proposed procedure becomes

$$u_m(\rho,\phi)=\sum_{n=-N}^{N}\left(a_n^{(m)}R_{n,m}^{(1)}(\rho)+b_n^{(m)}R_{n,m}^{(2)}(\rho)\right)e^{in\phi}, \tag{2}$$

for $m=1,2$. In the outermost region, instead of u_0, the scattered field $u_s=u_0-u_i$ is represented by this series for $m=0$. Here, N is a sufficiently large number and $a_n^{(m)}$, $b_n^{(m)}$ are unknown coefficients to be determined.

2.1. Derivation of the Coefficients of the General Solution

In order to determine the coefficients $a_n^{(m)}$, $b_n^{(m)}$ in Eq. (2), a linear system of equations for each of the boundaries Γ_1 and Γ_2 is obtained by applying the procedure given in [13, 16]. Briefly, after imposing the boundary conditions $u_{m-1}=u_m$ and $\partial_\rho u_{m-1}=\partial_\rho u_m$ on Γ_m, $m=1,2$, the functions $R_{n,m}^{(1)}$, $R_{n,m}^{(2)}$ and their radial derivatives are expanded into Fourier series. Then, we apply an inner product with $e^{-ip\phi}$, $p=-N,\ldots,N$, on both sides of the boundary conditions by using the definition given in [16] for the inner product. In virtue of the orthogonality of complex exponentials, two linear systems of equations

$$\begin{bmatrix}\mathbf{Z_1^{1,(0)}} & \mathbf{Z_1^{2,(0)}} & -\mathbf{Z_1^{1,(1)}} & -\mathbf{Z_1^{2,(1)}}\\ \mathbf{Z_1^{3,(0)}} & \mathbf{Z_1^{4,(0)}} & -\mathbf{Z_1^{3,(1)}} & -\mathbf{Z_1^{4,(1)}}\end{bmatrix}\begin{bmatrix}\mathbf{A^{(0)}}\\ \mathbf{B^{(0)}}\\ \mathbf{A^{(1)}}\\ \mathbf{A^{(1)}}\end{bmatrix}=\begin{bmatrix}\mathbf{W}\\ \hat{\mathbf{W}}\end{bmatrix} \tag{3}$$

and

$$\begin{bmatrix}\mathbf{Z_2^{1,(1)}} & \mathbf{Z_2^{2,(1)}} & -\mathbf{Z_2^{1,(2)}} & -\mathbf{Z_2^{2,(2)}}\\ \mathbf{Z_2^{3,(1)}} & \mathbf{Z_2^{4,(1)}} & -\mathbf{Z_2^{3,(2)}} & -\mathbf{Z_2^{4,(2)}}\end{bmatrix}\begin{bmatrix}\mathbf{A^{(1)}}\\ \mathbf{B^{(1)}}\\ \mathbf{A^{(2)}}\\ \mathbf{A^{(2)}}\end{bmatrix}=\mathbf{0} \tag{4}$$

are obtained for boundaries Γ_1 and Γ_2, respectively. Here, $\mathbf{W}$, $\hat{\mathbf{W}}$, $\mathbf{A^{(m)}}$, and $\mathbf{B^{(m)}}$, $m=0,1,2$, are column vectors of size $(2N+1)$. The elements of $\mathbf{A^{(m)}}$ and $\mathbf{B^{(m)}}$ are the unknown coefficients $a_n^{(m)}$ and $b_n^{(m)}$, respectively, and

$$\mathbf{W}=\left[\left\langle u_i,e^{-i(-N)\phi}\right\rangle\quad\left\langle u_i,e^{-i(-N+1)\phi}\right\rangle\quad\ldots\quad\left\langle u_i,e^{-i(N-1)\phi}\right\rangle\quad\left\langle u_i,e^{-i(N)\phi}\right\rangle\right]^T, \tag{5}$$

$$\hat{\mathbf{W}}=\left[\left\langle \partial_\rho u_i,e^{-i(-N)\phi}\right\rangle\quad\left\langle \partial_\rho u_i,e^{-i(-N+1)\phi}\right\rangle\quad\ldots\quad\left\langle \partial_\rho u_i,e^{-i(N-1)\phi}\right\rangle\quad\left\langle \partial_\rho u_i,e^{-i(N)\phi}\right\rangle\right]^T. \tag{6}$$

The coefficient matrices of Eqs. (3) and (4) contain $(2N+1)\times(2N+1)$ submatrices

$$\mathbf{Z_m^{t,(j)}} = \begin{bmatrix} C^{t,(j)}_{2N,-N,m} & C^{t,(j)}_{2N-1,-N+1,m} & \cdots & C^{t,(j)}_{0,N,m} \\ C^{t,(j)}_{2N-1,-N,m} & C^{t,(j)}_{2N-2,-N+1,m} & \cdots & C^{t,(j)}_{-1,N,m} \\ \vdots & \vdots & \ddots & \vdots \\ C^{t,(j)}_{0,-N,m} & C^{t,(j)}_{-1,-N+1,m} & \cdots & C^{t,(j)}_{-2N,N,m} \end{bmatrix} \tag{7}$$

whose elements are the Fourier coefficients

$$C^{t,(j)}_{q,n,m} = \frac{1}{2\pi}\int_0^{2\pi} R^{(t)}_{n,j}\left(f_m\left(\phi\right)\right) e^{-iq\phi}\, d\phi. \tag{8}$$

In Eq. (8), $R^{(3)}_{n,j} = \partial_\rho R^{(1)}_{n,j}$ and $R^{(4)}_{n,j} = \partial_\rho R^{(2)}_{n,j}$.

Applying the Sommerfeld radiation condition yields $\mathbf{A^{(0)}} = \mathbf{0}$. Similarly, $\mathbf{B^{(2)}}$ vanishes since in the homogeneous core $R^{(2)}_{n,2}(\rho)$ is equal to $H^{(1)}_n(k_2\rho)$, which is singular at the origin. The details of the above procedure are given in [13, 16]. In the present formulation, more generalized functions, i.e., $R^{(1)}_{n,m}$ and $R^{(2)}_{n,m}$, are used to represent the total field, and accordingly the Fourier coefficients in Eq. (7) are modified.

2.1.1. The Explicit Expressions for Coefficients of the General Solution

One can extract the unknown coefficients from the linear systems in Eqs. (3) and (4), and obtain their explicit expressions as

$$\mathbf{B^{(0)}} = \left(\tilde{\mathbf{Z}}_\mathbf{1}\right)^{-1}\left(\hat{\mathbf{W}} - \mathbf{\Psi_2}\left(\mathbf{\Psi_1}\right)^{-1}\mathbf{W}\right) \tag{9}$$

$$\mathbf{A^{(1)}} = \left(\mathbf{\Psi_1}\right)^{-1}\left(-\mathbf{Z_1^{2,(0)}}\mathbf{B^{(0)}} - \mathbf{W}\right) \tag{10}$$

$$\mathbf{B^{(1)}} = -\left(\tilde{\mathbf{Z}}_\mathbf{2}^\mathbf{2}\right)^{-1}\tilde{\mathbf{Z}}_\mathbf{2}^\mathbf{1}\mathbf{A^{(1)}} \tag{11}$$

$$\mathbf{A^{(2)}} = \left(\mathbf{Z_2^{1,(2)}}\right)^{-1}\left(\mathbf{Z_2^{1,(1)}}\mathbf{A^{(1)}} + \mathbf{Z_2^{2,(1)}}\mathbf{B^{(1)}}\right) \tag{12}$$

where

$$\tilde{\mathbf{Z}}_\mathbf{1} = \mathbf{\Psi_2}\left(\mathbf{\Psi_1}\right)^{-1}\mathbf{Z_1^{2,(0)}} - \mathbf{Z_1^{4,(0)}} \tag{13}$$

$$\mathbf{\Psi_j} = \mathbf{Z_1^{2j,(1)}}\left(\tilde{\mathbf{Z}}_\mathbf{2}^\mathbf{2}\right)^{-1}\tilde{\mathbf{Z}}_\mathbf{2}^\mathbf{1} - \mathbf{Z_1^{2j-1,(1)}}, \quad j=1,2 \tag{14}$$

$$\tilde{\mathbf{Z}}_\mathbf{2}^\mathbf{j} = \mathbf{Z_2^{3,(2)}}\left(\mathbf{Z_2^{1,(2)}}\right)^{-1}\mathbf{Z_2^{j,(1)}} - \mathbf{Z_2^{2+j,(1)}}, \quad j=1,2 \tag{15}$$

When the core layer is a perfect electric conductor (PEC), $\mathbf{A^{(2)}}$ and $\mathbf{B^{(2)}}$ vanish, and Eq. (15) transforms into $\tilde{\mathbf{Z}}_\mathbf{2}^\mathbf{j} = \mathbf{Z_2^{j,(1)}}$, $j=1,2$.

2.2. The Explicit Expressions of $\mathbf{R^{(1)}_{n,m}}$ and $\mathbf{R^{(2)}_{n,m}}$ for Special Profiles

In free-space and the homogeneous core, $R^{(1)}_{n,m}(\rho) = J_n(k_m\rho)$ and $R^{(2)}_{n,m}(\rho) = H^{(1)}_n(k_m\rho)$, $m=0,2$. The explicit expressions of $R^{(1)}_{n,m}$ and $R^{(2)}_{n,m}$ are given below for some radially inhomogeneous layers that have different dielectric permittivity profiles [3–5].

- Profile 1:

$$\varepsilon_1\left(\rho\right) = \varepsilon_0\frac{C}{\left(k_0\rho\right)^2} \tag{16}$$

$$R^{(1)}_{n,1}\left(\rho\right) = \left(k_0\rho\right)^{1+p} \tag{17}$$

$$R^{(2)}_{n,1}\left(\rho\right) = \left(k_0\rho\right)^{1-p} \tag{18}$$

Here, C is a complex parameter and $p^2 = n^2 - C$.

- *Profile 2:*

$$\varepsilon_1(\rho) = \varepsilon_0 \alpha^2 \rho^{2\beta}, \quad \beta \neq -1 \tag{19}$$

$$R_{n,1}^{(1)}(\rho) = J_\nu\left(\frac{\alpha k_0}{\beta+1}\rho^{\beta+1}\right) \tag{20}$$

$$R_{n,1}^{(2)}(\rho) = Y_\nu\left(\frac{\alpha k_0}{\beta+1}\rho^{\beta+1}\right) \tag{21}$$

Here, α and *beta* are complex and real parameters, respectively, while Y_ν is the Neumann function of order ν, and $\nu = |n|/(\beta+1)$. Note that, C in Eq. (16) and α in Eq. (19) will be real for lossless profiles.

3. NUMERICAL RESULTS

Some numerical simulations have been performed for two different-shaped objects that have various dielectric permittivity distributions. In these simulations, the objects are illuminated by a TM plane wave at 300 MHz with an angle of $\pi/4$ with respect to the x-axis. By using a PC with a 3.40 GHz CPU and 12 GB of RAM, the scattered field is computed on a 2 m-radius circle whose center is at the origin. The results are compared with the ones obtained by using MoM. While the cell size in MoM is chosen in terms of the minimum wavelength $\lambda_{\min}$ as $\lambda_{\min}/14 \times \lambda_{\min}/14$, the truncation number N in the proposed method is chosen as 50 (a discussion on the interval of N for which convergent results are achieved is given in [17]).

In the first example, a V-notched circular radially inhomogeneous layer surrounding a homogeneous circular core is considered. Three different cases in which $\varepsilon_1(\rho)$ is proportional to $1/rho^2$, $1/rho$ and ρ, have been designed by using the profiles in Eqs. (16) and (19). More explicitly,

- *Case 1:* $C = 50 + 3i$ in *Profile 1*, and $\varepsilon'_{r2} = 14$, $\sigma_2 = 0.03\,\mathrm{S/m}$;
- *Case 2:* $\alpha^2 = 15/k_0 + 0.3i$, $\beta = -0.5$ in *Profile 2*, and $\varepsilon'_{r2} = 8$, $\sigma_2 = 0.05\,\mathrm{S/m}$;
- *Case 3:* $\alpha^2 = 25/k_0 + 0.06i$, $\beta = 0.5$ in *Profile 2*, and $\varepsilon'_{r2} = 4$, $\sigma_2 = 0.05\,\mathrm{S/m}$.

where ε'_{r2} is the real part of the complex relative permittivity, and σ_2 is the conductivity of the core. The real parts of the corresponding complex relative permittivity distributions are given in Fig. 2. The conductivity distributions are not given here since they have the same radial behavior with the permittivities in the radially inhomogeneous layer. They change in the intervals $[1.3, 14.1]$ (mS/m), $[5.0, 16.7]$ (mS/m) and $[0.3, 1.0]$ (mS/m) for *Case 1*, *Case 2* and *Case 3*, respectively.

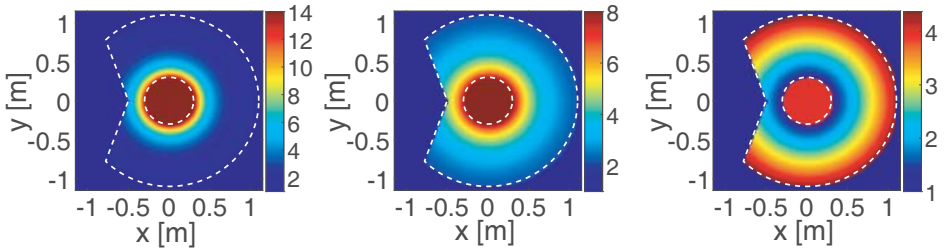

Figure 2. Real part of the complex relative permittivity distribution of a V-notched circular object with a radially inhomogeneous layer surrounding a circular core: (a) *Case 1*, (b) *Case 2*, (c) *Case 3*.

The amplitude and phase of the scattered fields obtained via the proposed method and MoM are very close to each other as shown in Fig. 3. During the implementation of MoM, the object is discretized as described above into 8932, 5055 and 2768 cells for *Case 1*, *Case 2* and *Case 3* respectively. For these cases, the computational advantage of the proposed approach is clearly seen in Table 1, where the computational times of the two methods are compared.

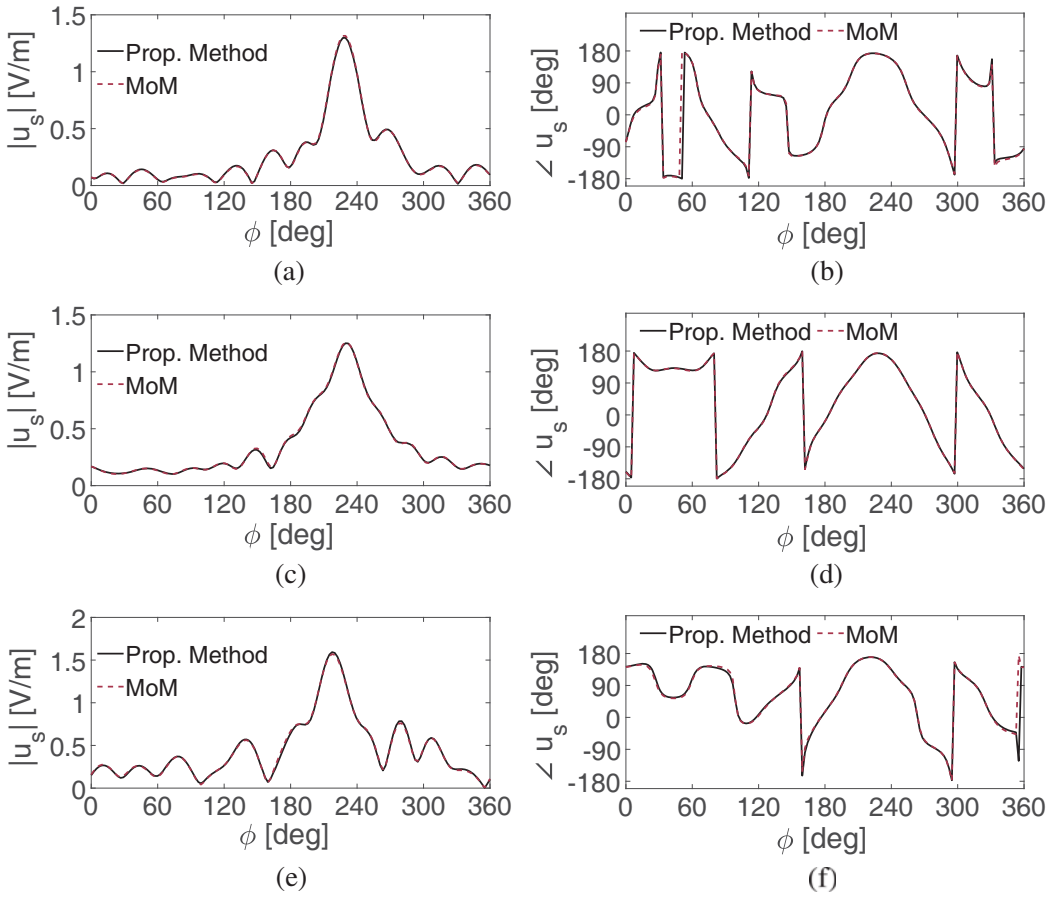

Figure 3. Comparison of the fields scattered from a V-notched circular object with a radially inhomogeneous layer surrounding a circular core: (a) amplitude and (b) phase for *Case 1*, (c) amplitude and (d) phase for *Case 2*, (e) amplitude and (f) phase for *Case 3*.

Table 1. Computational times for *Case 1*, *Case 2* and *Case 3*.

	Case 1	*Case 2*	*Case 3*
Time for Proposed Method (s)	0.5	1.2	0.9
Time for MoM (s)	83.9	21.2	5.9

In order to test the accuracy of the proposed method inside the object, we have computed the total field on a 0.4 m-radius circle, which lies in the radially inhomogeneous layer, for *Case 3*. As seen in Figs. 4(a) and 4(b), the proposed method yields satisfactory results. As a final simulation for this example, the dielectric core in *Case 3* has been replaced by a PEC. The proposed method continues to yield accurate results, and the scattered field in Figs. 3(e) and 3(f) transforms into the one given in Figs. 4(c) and 4(d).

In the second example, the proposed approach has been tested on a rectangular radially inhomogeneous object with a non-circular hole. As in the first example, three basic radial dependencies has been considered, i.e., $\varepsilon_1(\rho)$ is proportional to $1/rho^2$, $1/rho$ and ρ. Accordingly,

- *Case 4:* $C = 80 + 3i$ in *Profile 1*, and $\varepsilon_2 = \varepsilon_0$;
- *Case 5:* $\alpha^2 = 20/k_0 + 0.3i$, $\beta = -0.5$ in *Profile 2*, and $\varepsilon_2 = \varepsilon_0$;
- *Case 6:* $\alpha^2 = 15/k_0 + 0.3i$, $\beta = 0.5$ in *Profile 2*, and $\varepsilon_2 = \varepsilon_0$.

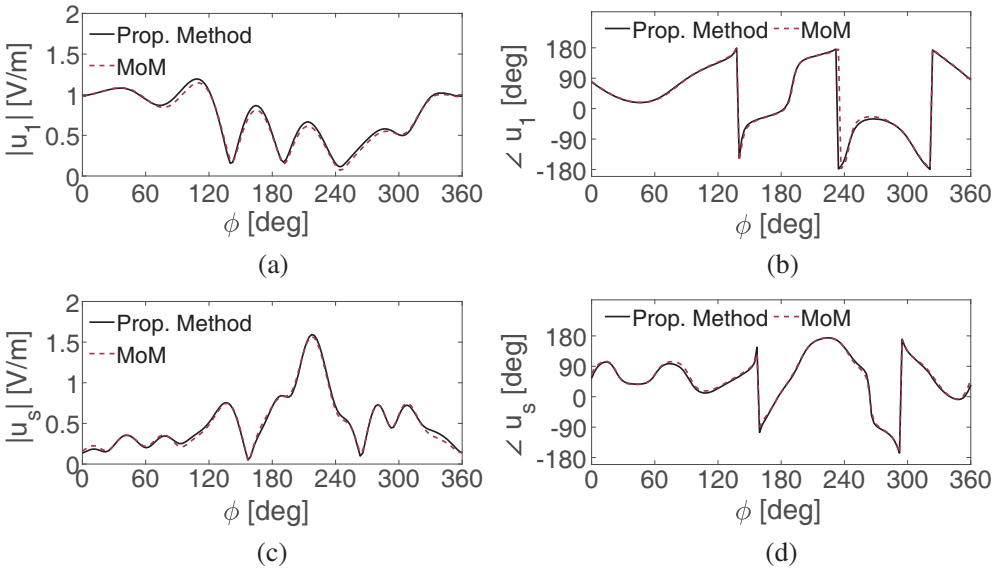

Figure 4. Comparison of the (a) amplitude and (b) phase of the total fields in radially inhomogeneous layer for *Case 3*. Comparison of the (c) amplitude and (d) phase of the scattered fields when the core in *Case 3* is replaced by a PEC.

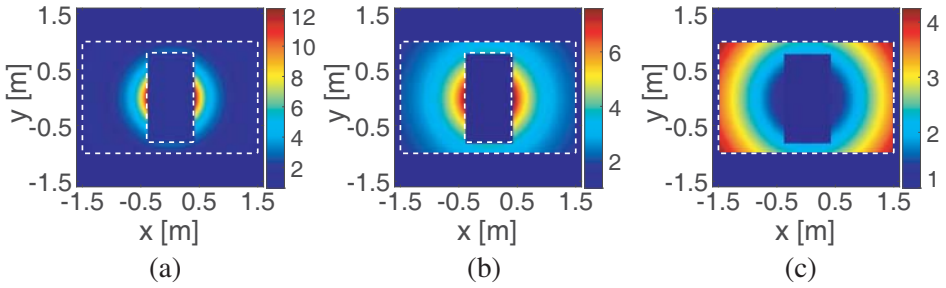

Figure 5. Real part of the complex relative permittivity distribution of a rectangular radially inhomogeneous object with a non-circular hole: (a) *Case 4*, (b)*Case 5*, (c) *Case 6*.

have been designed. Fig. 5 illustrates the real parts of the corresponding complex relative permittivity distributions. As to the conductivities in the radially inhomogeneous layer, they change in the intervals $[0.4, 7.9]$ (mS/m), $[2.8, 12.5]$ (mS/m) and $[2.0, 9.0]$ (mS/m) for *Case 1*, *Case 2* and *Case 3*, respectively.

As seen in Fig. 6, the scattered field has been accurately computed via the proposed method for this relatively complex-shaped object, which has boundaries with corners. For this example, only the radially inhomogeneous layer is discretized in MoM. The resulting cell numbers are 11780, 7306 and 3988 for *Case 4*, *Case 5* and *Case 6*, respectively. As seen in Table 2, the computational advantage of the proposed method becomes more substantial as the number of mesh cells required during the implementation of MoM increases. On the other hand, the method tends to lose accuracy for complex shaped objects whose boundaries have large and frequent variations, as discussed in [13, 17].

Table 2. Computational times for *Case 4*, *Case 5* and *Case 6*.

	Case 4	*Case 5*	*Case 6*
Time for Proposed Method (s)	0.5	1.4	1.2
Time for MoM (s)	139.6	42.5	11.6

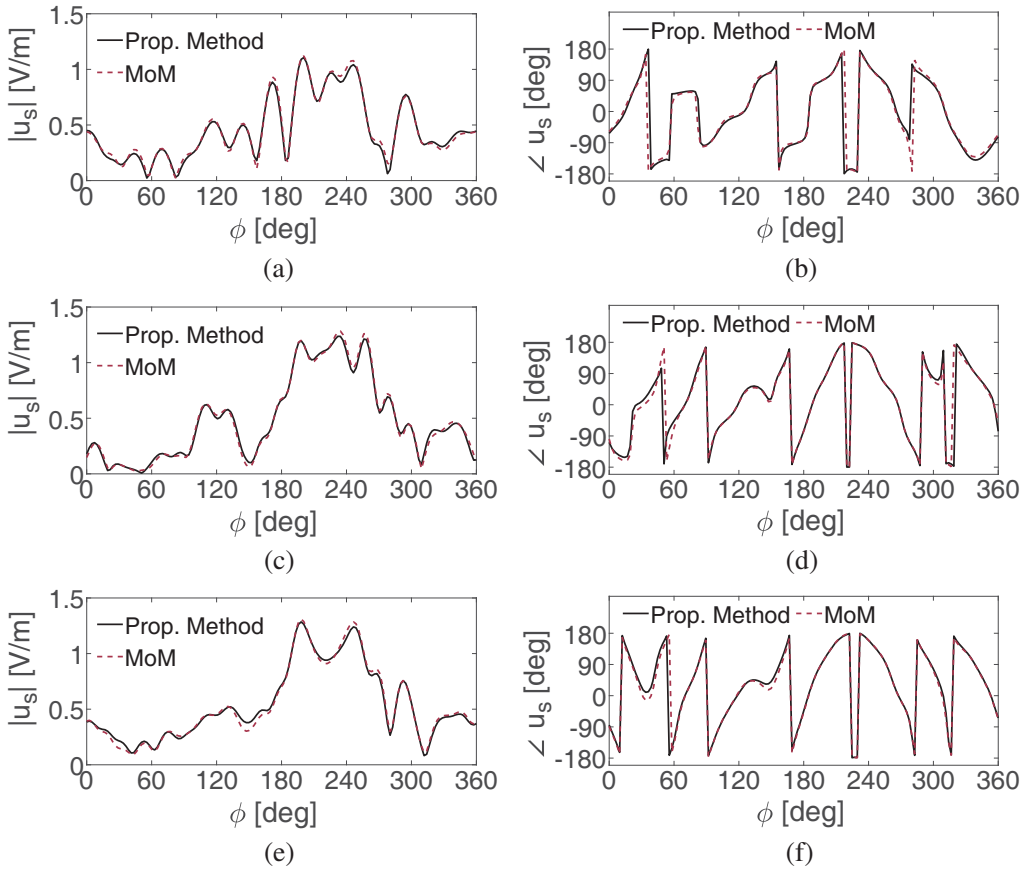

Figure 6. Comparison of the fields scattered from rectangular radially inhomogeneous object with a non-circular hole: (a) amplitude and (b) phase for *Case 4*, (c) amplitude and (d) phase for *Case 5*, (e) amplitude and (f) phase for *Case 6*.

3.1. Energy Conservation

It can also be shown that energy conservation is satisfied when the fields are computed via the proposed method. Energy conservation implies

$$W_e = W_a + W_s \tag{22}$$

where W_e, W_a, and W_s are respectively the extinction power, absorbed power, and scattered power per unit length of the cylinder [18]. More explicitly,

$$W_s = \frac{1}{2} \oint_{\partial\Omega} \mathrm{Re}\left(\mathbf{E_s} \times \mathbf{H_s^*}\right) \cdot \hat{\mathbf{n}}\, ds, \tag{23}$$

$$W_e = -\frac{1}{2} \oint_{\partial\Omega} \mathrm{Re}\left(\mathbf{E_i} \times \mathbf{H_s^*} + \mathbf{E_s} \times \mathbf{H_i^*}\right) \cdot \hat{\mathbf{n}}\, ds \tag{24}$$

where $\partial\Omega$ is the boundary of a region Ω containing the object on the $\rho\phi$-plane, and $\hat{\mathbf{n}}$ is the unit outward normal vector on $\partial\Omega$ [19]. $\mathbf{E_s}$ and $\mathbf{H_s}$ are the scattered electric and magnetic field vectors while $\mathbf{H_i}$ is the incident magnetic field vector. The absorbed power can be computed by

$$W_a = \frac{1}{2} \iint_{\Omega} \sigma\left(\rho\right) |\mathbf{E}|^2\, dA \tag{25}$$

Here, $\mathbf{E}$ is the total electric field vector, and σ is the conductivity in Ω.

We have chosen $\partial\Omega$ as a 2 m-radius circle and repeated all of the above given simulations individually for 100 equally spaced incidence angles, ϕ_i, in the interval $[0, 2\pi)$. It has been observed that the computed

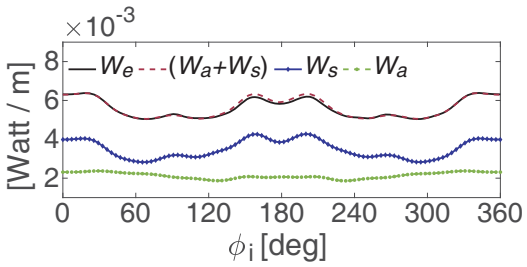

Figure 7. Comparison of the extinction power W_e, the scattered power W_s and the absorbed power W_a for *Case 1*.

fields consistently satisfy Eq. (22). As an example, W_s, W_a, W_e and $W_a + W_s$ for *Case 1* are given in Fig. 7.

3.2. Reciprocity

Finally, we have tested whether the computed fields satisfy the Lorentz reciprocity theorem, which is

$$\oint_{\partial\Omega} (\mathbf{E_A} \times \mathbf{H_B}) \cdot \hat{\mathbf{n}}\, ds = \oint_{\partial\Omega} (\mathbf{E_B} \times \mathbf{H_A}) \cdot \hat{\mathbf{n}}\, ds \tag{26}$$

in source-free region. Here, $\mathbf{E_A}$, $\mathbf{H_A}$ and $\mathbf{E_B}$, $\mathbf{H_B}$ are the fields due to sources A and B, respectively. For the purpose of numerical validation of Eq. (26), *Case 1* has been considered. The fields $\mathbf{E_A}$ and $\mathbf{H_A}$ have been computed for an incidence angle of $\phi_A = 0$ while $\mathbf{E_B}$ and $\mathbf{H_B}$ have been computed individually for 100 equally spaced incidence angles, ϕ_B, in the interval $[0, 2\pi)$. The satisfaction of Eq. (26) is shown in Fig. 8 where I_{AB} and I_{BA} are the left and right hand sides of Eq. (26).

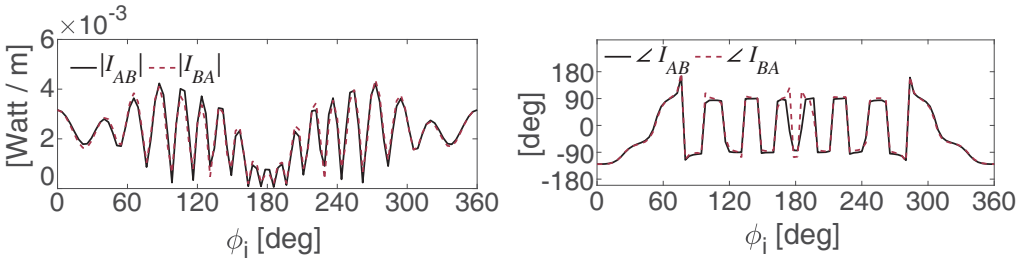

Figure 8. Comparison of (a) $|I_{AB}|$ and $|I_{BA}|$, (b) $\angle I_{AB}$ and $\angle I_{BA}$.

4. CONCLUSION

The proposed method can be used for fast computation of the field scattered from radially inhomogeneous circular cylinders with deformations such as notches, grooves, noncircular hollows, etc. It is also applicable for multilayer cylinders that have one or more radially inhomogeneous layers around an arbitrary shaped dielectric or PEC core. Based on the results related to the basic dielectric permittivity profiles given here, we expect that the proposed method will be beneficial for different $\varepsilon_1(\rho)$ profiles (including lossy ones), as long as functions $R^{(1)}_{n,m}$, $R^{(2)}_{n,m}$ are determined.

The time and memory complexities of the proposed method are $\mathcal{O}(N^3)$ and $\mathcal{O}(N^2)$ while they are $\mathcal{O}(N^3_{MoM})$ and $\mathcal{O}(N^2_{MoM})$ for MoM. Here N_{MoM} is the number of mesh cells required by MoM. Except objects with small electrical sizes, mostly $N < N_{MoM}$ and the proposed method is more advantageous in terms of time and memory complexities.

Adaptation of the method to the oblique incidence case constitutes a part of our future work. The possibility of extending the method to more general inhomogeneity profiles involving azimuthal variations will also be investigated.

REFERENCES

1. El-Galy, I. M., B. I. Saleh, and M. H. Ahmed, "Functionally graded materials classifications and development trends from industrial point of view," *SN Appl. Sci.*, Vol. 1, 1378, 2019.
2. Westcott, B. S., "Electromagnetic wave propagation in cylindrically stratified isotropic media," *Electronics Letters*, Vol. 4, No. 16, 323–324, 1968.
3. Burman, R., "Electromagnetic scattering by a cylinder with an inhomogeneous sheath," *Electronics Letters*, Vol. 2, No. 2, 66–67, 1966.
4. Yeh, C. and Z. A. Kaprielian, "Scattering from a cylinder coated with an inhomogeneous dielectric sheath," *Canadian Journal of Physics*, Vol. 41, 143–151, 1963.
5. Samaddar, S. N., "Scattering of plane electromagnetic waves by radially inhomogeneous infinite cylinders," *Il Nuovo Cimento B*, Vol. 66, No. 1, 33–50, 1970.
6. Tsalamengas, J., "Oblique scattering from radially inhomogeneous dielectric cylinders: An exact Volterra integral equation formulation," *Journal of Quantitative Spectroscopy and Radiative Transfer*, Vol. 213, 62–73, 2018.
7. Kai, L. and A. D'Alessio, "Finely stratified cylinder model for radially inhomogeneous cylinders normally irradiated by electromagnetic plane waves," *Applied Optics*, Vol. 34, No. 24, 5520–5530, 1995.
8. Kiani, M., A. Abdolali, and M. M. Salary, "Analysis of scattering from cylindrical structures coated by radially inhomogeneous layer using Taylor's series method," *Journal of Electromagnetic Waves and Applications*, Vol. 28, No. 13, 1642–1660, 2014.
9. Jarem, J. M., "Rigorous coupled wave analysis of radially and azimuthally-inhomogeneous, elliptical, cylindrical systems," *Progress In Electromagnetics Research*, Vol. 34, 89–115, 2001.
10. Watanabe, Y. and H. Sato, "Review fabrication of functionally graded materials under a centrifugal force," *Nanocomposites with Unique Properties and Applications in Medicine and Industry*, 133–150, edited by John Cuppoletti, IntechOpen, London, 2011.
11. Richmond, J. H., "Scattering by a dielectric cylinder of arbitrary cross section shape," *IEEE Trans. Antennas Propag.*, Vol. 13, No. 3, 334–341, 1965.
12. Jin, J. M. and V. V. Liepa, "Application of hybrid finite element method to electromagnetic scattering from coated cylinders," *IEEE Trans. Antennas Propag.*, Vol. 36, No. 1, 50–54, 1988.
13. Aslanyürek, B. and T. U. Gürbüz, "A continuity-based series solution for electromagnetic scattering by arbitrary shaped multilayer cylinders: TM case," *IEEE Trans. Antennas Propag.*, Vol. 65, No. 2, 812–819, 2017.
14. Yao, S., C. Cheng, Z. Hu, and Z. Niu, "Investigation of singularity orders and eigen-angular functions for V-notches in radially inhomogeneous materials," *Mechanics of Advanced Materials and Structures*, Vol. 25, No. 4, 295–303, 2016.
15. Wang, W., H. Yuan, X. Li, and P. Shi, "Stress concentration and damage factor due to central elliptical hole in functionally graded panels subjected to uniform tensile traction," *Materials*, Vol. 12, No. 3, 422, 2019.
16. Aslanyürek, B. and T. U. Gürbüz, "An efficient recursive approach for electromagnetic scattering by arbitrary-shaped multilayer cylinders," *IEEE Antennas Wireless Propag. Lett.*, Vol. 19, No. 8, 1375–1379, 2020.
17. Aslanyürek, B. and T. U. Gürbüz, "A series solution for TE electromagnetic scattering by arbitrary shaped multilayer cylinders," *IEEE Antennas Wireless Propag. Lett.*, Vol. 17, No. 1, 38–41, 2018.
18. Mishchenko, M. I., L. D. Travis, and A. A. Lacis, *Scattering, Absorption, and Emission of Light by Small Particles*, Cambridge Univ. Press, Cambridge, 2002.
19. Frezza, F., F. Mangini, and N. Tedeschi, "Introduction to electromagnetic scattering: Tutorial," *J. Opt. Soc. Am. A*, Vol. 35, 163–173, 2018.